

MAE/ECE 535: Design of Electromechanical Systems  
Design Report

---

**Electro-Permanent Magnetic Clamp for  
Workpiece Holding During Machining**

**Evan Grant, Auston Gray, Stephen Griffith, Larry Thomas**

April 23, 2020

---

## Abstract

Workpiece holding is a challenge unique to every machining situation. Magnetic chucks are an enticing alternative to conventional clamps. In this vein, Electro-Permanent Magnet Clamps (EPMCs) offer the promise of strong clamping forces when turned on, low clamping force when turned off, with the benefit of not adding heat to the workpiece. This report will detail the process of designing an Electro-Permanent Magnetic Clamp to meet certain design requirements. The design featured three NdFeB magnets and two AlNiCo magnets around two poles. The AlNiCos could be switched using an electromagnet to turn clamping on and off. The process began with simple MCA analysis of the clamp, followed by refining the design with 2D FEMM simulation of the design. Calculations were performed to determine the necessary circuitry and current to flip the AlNiCo magnets, as well as the heat produced during the flip. Finally, results were optimized through 3D simulation in ANSYS. The design was able to produce a 500 lb clamping force with a factor of safety of 3 while maintaining a residual force of under 10 lbs. Analysis of the circuitry and heat transfer showed that only a minimal increase in temperature would result from powering the coils to flip the AlNiCo Magnets. This is crucial so as not to distort the workpiece with heat. In the end, the design yielded a very economical alternative to conventional clamping.

## Introduction

Conventional clamps have many advantages, but they are often bulky and limited to securely holding a few specific workpiece geometries. The emerging technology of Electro-Permanent Magnetic Clamps allows for reduced risk of failure as well as reduced heat when compared to electromagnet clamps. The design of EPMCs relies on precise manipulation of the properties of magnets and ferromagnetic materials to provide impressive performance and a reasonable price. This design project sought to optimize the design of an example EPMC constrained to two 50 mm by 50 mm poles. The goal of this project was to find a theoretical design which would be able to hold a workpiece with 500 lbs of clamping force with a preferred safety factor of 3, while maintaining reasonably low force in the off configuration. The design of electromechanical systems is complex and involved, so this paper will describe multiple analysis techniques that were taken to design, refine, and analyse the EPMC. The work performed in this project was extensive, so the results are not without merit.

## Magnetic Circuit Analysis

Magnetic circuit analysis was employed for the EPMC because it provides a quick way to estimate magnetic forces. Because MCA is much less computationally expensive and time consuming than finite element analysis methods, this technique was used to systematically vary parameters and observe how they affected the provided clamping force in the on and off configurations to guide design decisions.

First, a magnetic circuit was constructed for the clamp in the on configuration, and it is shown below in Figure 1. The unknown fluxes were labeled in each branch of the circuit, and the unknown MMF values across each element were labeled on the circuit. A similar circuit with reversed directions of  $\Phi_3$  was used to calculate magnetic force in the off configuration.

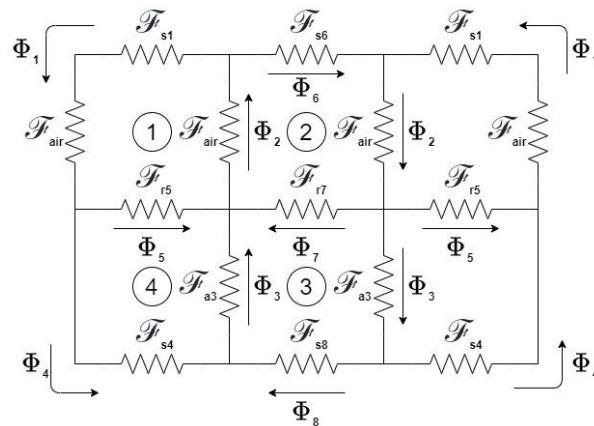
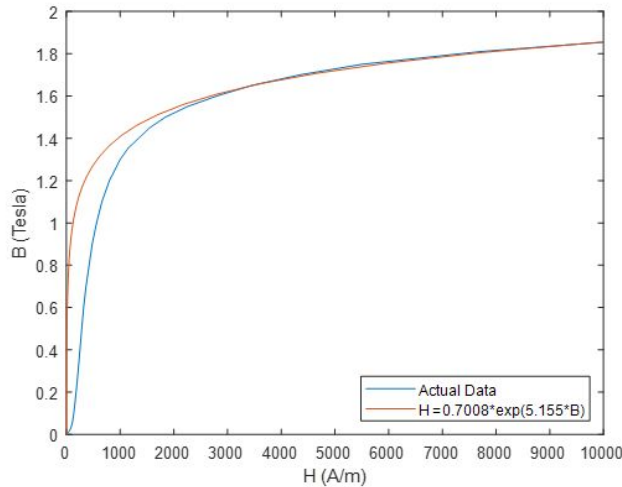


Figure 1 - Magnetic Circuit in the On Configuration

The steel sections were originally neglected from the MCA analysis because they had much lower reluctances than air, but this assumption prevented the analysis from converging to a solution. The steel elements

provided important drops in MMF that caused loops in the circuit to have a net 0 MMF. Next, an iterative approach was used to loop through different magnetic flux combinations in the circuit and find which combination resulted in 0 MMF around the loops in the circuit. This approach accounted for the nonlinear B-H behavior of the steel and magnets using B-H curves implemented in MATLAB, but it was inefficient and time consuming. Finally, the B-H curves were assumed to behave linearly for the magnets and the steel. This simplified the analysis considerably, but led to flux densities in steel elements around 3 Tesla, indicating that linear assumption for the steel did not hold.

For the final MCA analysis, an approximate linear B-H equation was found for the magnets. This linear assumption was reasonable because the B-H curves for both magnets were approximately linear above the knees in the curve [1,2]. In order to account for the nonlinear B-H relationship for steel, an exponential trendline was fit to the B-H curve for 1020 steel as shown in Figure 2 below [3]. This grade of steel was selected because it has a similar chemical composition to 1025 steel, and the physical properties are more readily available. These B-H relationships were used to relate the flux through each circuit element to the MMF of each element.



**Figure 2 - Actual and Modeled B-H Curve for 1020 Steel 31]**

In the circuit, the magnetic fluxes are the 8 unknowns that are to be solved, and 8 linearly independent equations are needed. Four of these equations come from the analogous Kirchoff's Current Law for magnetic flux, which states that the sum of electrical currents, or in the magnetic case, fluxes must equal zero. The other 4 equations come from knowing that the MMF around any 4 closed circuit loops must equal zero. The MMF of each element is calculated based on the relationship  $\mathcal{F} = H * l = \mathcal{R} * \Phi$  as illustrated on Table 1 below. The complete system of equations for the system is provided in Appendix A.

**Table 1 - MMF Calculations for Circuit Elements**

Element Type	B-H relationship	MMF
Air	$B = \mu_0 H$	$\mathcal{F}_{air} = \frac{l_{air}}{\mu_0 A_{air}} * \Phi$
AlNiCo Magnets	$B = 3.513 * 10^{-6} H + 1.2037$	$\mathcal{F}_a = 284,656 * \frac{\Phi * l_a}{A_a} - 342,641 * l_a$
NdFeB Magnets	$B = 1.31 * 10^{-6} H + 1.35$	$\mathcal{F}_r = 284,656 * \frac{\Phi * l_r}{A_r} - 1,030,534 * l_r$
Steel	$H = 0.7008 * exp(5.155 B)$	$\mathcal{F}_s = 0.7008 * exp(5.155 * \frac{\Phi}{A_s}) * l_s$

The system of equations above is nonlinear with respect to flux, so the `vpsolve()` function in MATLAB was utilized to find a numerical solution. The overall force was determined applying the equation  $|F| = \Phi^2 / (2\mu_0 A_{gap})$  to each air gap and adding the forces together. An initial simulation was run with a clamp depth of 50 mm, a steel width of 25 mm, a NdFeB width of 25 mm and thickness of 5 mm, an AlNiCo width of 45 mm

and thickness of 7 mm. The force supplied by the clamp was 1,722 lbf in the on configuration and 26 lbf in the off configuration. To gain a better intuition about how different parameters affect the force results, MATLAB was used to systematically loop through and change different parameters.

First, the width of the magnets were varied. The AlNiCo magnet width was varied from 30 mm to 45 mm in 1 mm increments, and the NdFeB magnet width was varied from 15 to 25 mm in 1 mm increments. The on and off clamping forces were calculated for each combination and are provided in Appendix B below. The clamp provided the most pulling force when both magnets had the largest width. There is a balance between the width for minimum force. Large clamping forces in the off position occur when either the AlNiCo or NdFeB areas are too big.

Finally, the thickness of the AlNiCo magnet was varied from 1 to 14 mm and the NdFeB was varied from 1 to 10 mm while the widths of these magnets were kept at the original values. In the on position, increasing the thickness of both magnets results in the maximum clamping force, but varying AlNiCo thickness has more influence than varying NdFeB thickness as shown in Appendix B. The magnet thickness has little effect on the off holding force. Additionally, the AlNiCo magnets are much cheaper than the NdFeB magnets, so small NdFeB and large AlNiCo thickness are desirable [4]. The magnet grades and steel dimensions were fixed for the MCA analysis.

Although simple to solve, the MCA had several limitations. First, the reluctance of the steel poles was not considered. Saturation likely occurs here, which would lead to lower observed clamping forces. Also, steel cross section areas and mean path lengths were estimated, and the uncertainty of these values could affect result accuracy. Finally, the air gap between the workpiece and the clamp was arbitrarily assumed to be 0.1 mm, and it could lead to inaccurate force values when the actual device operates with no air gap. The analysis also did not take into account the effects of fringing and non constant flux distributions across cross section areas.

### FEMM Analysis

Along with performing the MCA, FEMM Finite Element Analysis software was utilized to examine the magnetic flux densities and magnetic forces in the EPMC. This analysis technique is more accurate than MCA because it accounts for the geometry of the clamp, saturation in steel poles, and fringing effects that were absent in the MCA. In order to solve for the magnetic reluctance force between the EPMC body and workpiece, FEMM required an air gap to exist between the components. Two simulations with air gaps of 0.05 mm and 0.1 mm were run, and the clamping forces in both trials were similar. A 0.1 mm air gap was used for all simulations because it reduced the number of elements needed and computation time in the simulation while providing accurate results.

Multiple simulations were run to vary different model parameters, and the results agreed with the MCA analysis. The largest width for both the AlNiCo and NdFeB magnets led to the highest reluctance forces in the on position and increasing the AlNiCo thickness improved clamping forces much more than increasing the NdFeB thickness. Additional simulations showed that increasing the steel width around the sides of the EPMC reduced saturation and led to higher clamping forces.

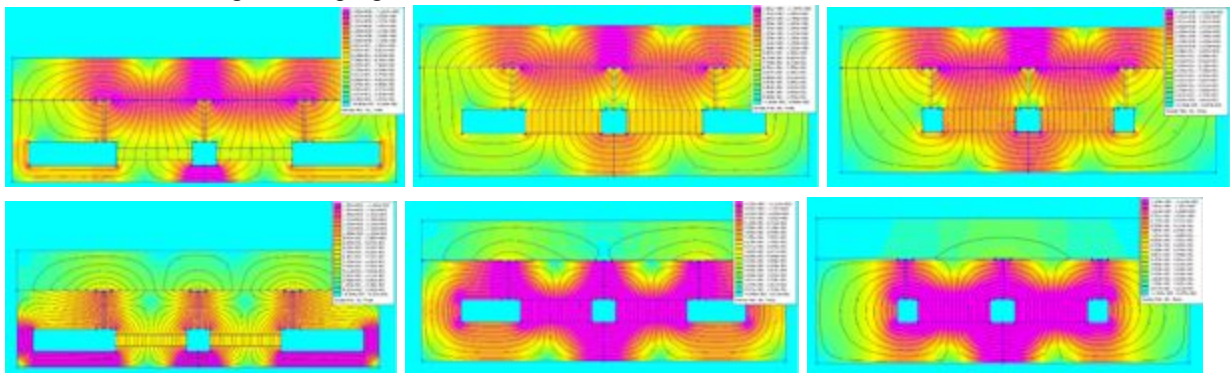


**Figure 3 - “On” and “Off” Configuration Flux Density Results for Selected FEMM Simulations**

Figure 3 above shows several designs considered. The design on the left has narrow steel sections around the sides and base of the clamp. These sections become saturated especially in the off configuration, leading to a lower on clamping force of 1258 lbf and high off clamping force of 109 lbf. The middle design had thicker steel edges which reduced saturation in the bottom of the clamp significantly in the on and off position, and the AlNiCo width was increased. The clamping force for this design was 1608 lbf and 32 lbf for the on and off configurations. Finally, the design was further optimized by changing the NdFeB material from N45 to N33 and the AlNiCo material from LNG 37 to LNG 56 and increasing the width of the steel on the sides. The stronger AlNiCo magnets

and weaker NdFeB magnets helped contain most of the magnetic flux density inside of the EPMC when in the off configuration, reducing the off force to 4.2 lbf. The clamping force was also slightly reduced to 1594 lbf. In order to maintain the geometric constraint of 60 mm between the poles, metal spacers were added between the thin NdFeB magnets and the steel body and poles. This allows a thin magnet to be used while providing a low reluctance path for the magnetic flux.

### Circuit Analysis

The functionality of the EPMC depends on the deliberate reversal of AlNiCo magnet polarity. To accomplish this, an impulse current must be supplied through the coils of wire surrounding the magnets to generate a magnetic field directly opposing them. The intensity of this generated magnetic field  $H$  must exceed the magnet's intrinsic coercivity  $H_{ci}$ . In a magnet's B-H curve, this point is visualized best as the point of greatest rate of change, and therefore where an externally-applied  $H$  will successfully "flip" magnet polarity. AlNiCo magnets are used in EPMC applications precisely because they demonstrate low intrinsic coercivity and can be flipped relatively easily. The magnets selected for use in this report are anisotropic cast AlNiCo 5, and their  $H_{ci}$  values are readily supplied by the manufacturer. These are the most common types of AlNiCo magnets because of their high magnetic performance relative to other AlNiCos, temperature resistance, and ability to be created at larger scales in more complex geometries. They have a preferred direction of magnetization, which can be flipped along this axis.

While a full analysis was conducted simultaneously for AlNiCo5 grades LNG34, LNG37, LNG40, LNG44, LNG52, and LNG60, this report will only highlight results for grade LNG44 which was ultimately selected. This grade is the most popular and resulted in a high performance EPMC while maintaining a lower  $H_{ci}$  (requiring less Amp-turns to repolarize) and reducing cost from the highest grades while maintaining a small volume required to fit inside the coil.. Its performance characteristics are given in Table 2.

**Table 2 - LNG44 Properties**

Grade	$H_{ci}$ [kA/m]	$B_r$ [T]
Alnico_LNG44	54	1.25

To proceed with circuit design, the product  $NI$  was determined. Here,  $N$  represents the number of turns in the coil and  $I$  represents the current being supplied through the coil. Their product is directly proportional to the  $H$  field within the solenoid. One approach to determine the relation would be to apply Ampere's Law which holds that (for solenoids),  $H = NI/l$ , where  $l$  is the length of the coil along its axis. However, this relation assumes the internal magnetic field generated is uniform throughout the length of the coil, which does not hold true for coils with low length-to-diameter ratios. The length of the coils surrounding the magnets in this application are limited to 0.012 m, and have an inner diameter approximately three times as large. Thus, another method must be utilized.

The Biot-Savart Law allows one to determine magnetic field intensity and direction at a specified point in space near a current-carrying conductor. Thus, it can be utilized to model a current-carrying loop of wire, which leads to the important relation:

$$H(x_p) = \frac{Ia^2}{2(a^2+x_p^2)^{3/2}}$$

Where  $a$  is the radius of the loop and  $x_p$  is the distance to a point P along the axis of the loop. In order to represent a coil with many wire loops, this expression must be integrated over the length of the coil using a differential current element  $I' = \frac{NI}{l}$ . Thus, the new equation becomes:

$$H(x_p) = \int_0^l \frac{I'a^2}{2(a^2+(x_p-x)^2)^{3/2}} dx = \frac{NI}{2l} \left( \frac{l-x_p}{\sqrt{a^2+(x_p-l)^2}} + \frac{x_p}{\sqrt{a^2+x_p^2}} \right)$$

Noting that the induced  $H$  field is most weak at each end of the solenoid,  $H(0)$  and  $H(l)$  must both experience an applied field greater than  $H_{ci}$ . Solving for  $H(0)$  results in:

$$H(0) = \frac{NI}{2\sqrt{a^2+l^2}}$$

Finally, substituting  $H(0) = H_{ci} = 54,000 \text{ A/m}$ ,  $a = 0.0301\text{m}$ ,  $l = 0.012\text{m}$ , and solving for  $NI$  yields  $3584.016 \text{ At}$ . However, in order to be certain the applied field will fully reverse the AlNiCo polarity, 200% of  $(NI)_{req}$  will be supplied to each coil. Therefore,  $NI = 7168.032 \text{ At}$ . A value for  $N$  can be determined by evaluating available space in the coil bobbin for many different wire sizes. It was assumed the coil could extend radially beyond the bobbin walls into the free space between the poles. AWG 22 copper magnet wire was ultimately selected because it is readily available, has low-profile insulation and low resistance compared to smaller wires. Using this gauge allows for 144 turns of wire per coil. Thus, the required current to flip magnet polarity is 49.78A. This value far exceeds the rated ampacity of AWG 22 copper wire (0.92A); however, this rating is an extremely conservative value from the National Electric Code and is based on insulator temperature over time under a long duration of steady current [6]. An impulse current of this magnitude was deemed acceptable - a decision later confirmed by heat transfer analysis using the exact system parameters.

The resistance of AWG 22 wire is 52.9392 Ohms/km, and the length of wire per coil is approximately 30.4128 m (from  $N \cdot \text{Perimeter}_{\text{coil}}$ ). Total resistance per coil is then expected to be 1.61003 Ohms. Given the required current of approximately 50A per coil, the required supplied voltage can be determined via Ohm's Law.  $V_{DC} = 49.78/1.61003 = 80.14\text{V}$ . Supplied voltage is 230VAC. Therefore, the circuit requires a transformer to step 230V down to the approx. 80V that is required by the coils, and then pass this AC current through a bridge rectifier to produce DC voltage at the corrected amplitude. This voltage will then be supplied to charge the capacitor bank prior to generating the current impulse. Because the two separate coils will be wired in parallel and current divides evenly among them, the total required current doubles while required voltage remains the same.

A capacitor bank was required because of this high power/current application ( $P = I^2R + L \frac{di}{dt}$  where  $\frac{di}{dt}$  is very large). Such a bank allows for extremely quick discharge rates, and total required energy storage was calculated by integrating the power expression over the duration of the impulse (calculated later) and relating it to the formula for potential energy storage in a capacitor ( $U = \frac{1}{2}CV^2$ ). The exact time response of the impulse was found by approximating coil inductance using an computed average flux density ( $B$ ) throughout the coil and applying the following equation:  $I_L = \frac{V}{R}(1 - e^{-t/\tau})$  where  $\tau = L/R$  and is the time constant. To be certain the impulse would be sufficient, the impulse was selected to last the duration of  $10\tau$ . Substituting all known values results in a  $\tau$  of 6.9ms and a total energy consumption of 560J. This defines a capacitor bank of at least 172mF at 80V.

### Heat Transfer Analysis

A transient heat transfer analysis was performed in ANSYS to ensure that the temperature increase due to joule heating of the wire windings did not damage the copper wire or affect the magnets. Two square solid copper rings with dimensions that matched those of the copper windings in the design were added to the ANSYS model for the EPMC. The heat generation feature was utilized to represent the resistive power losses due to the current in the copper wire and was calculated for each coil using the following equation:  $Q_{gen}(t) = I(t)^2R/V_{copper}$ , where  $Q_{gen}(t)$  represents the heat rate generated per unit volume. Since the current varies with time due to the inductance of the copper coils,  $Q_{gen}(t)$  was calculated at each simulation time step and uploaded to ANSYS.

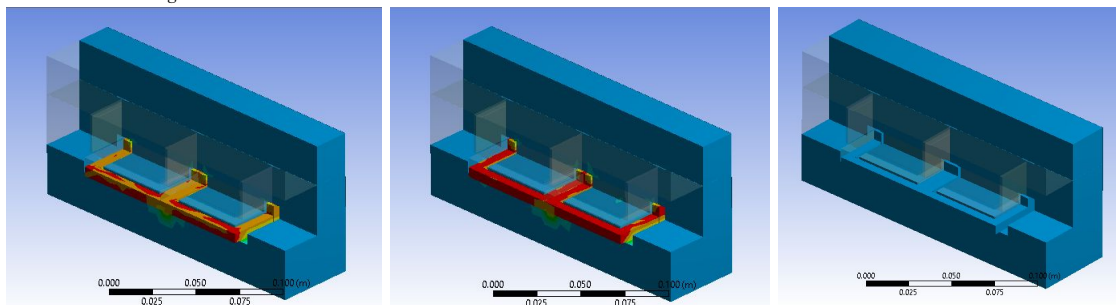


**Figure 4 - Results of Transient Heat Transfer Analysis**

Figure 4 above shows how the temperature in the clamp varies over time. In the leftmost simulation, all parts in the assembly were initially at 20 °C when the voltage was applied to the copper wire. At 6.1 ms as shown in the middle image, when the applied voltage is removed and the current begins to decay, the maximum temperature, which occurs in the copper, is 29.8 °C. The max temperature of the simulation, which occurred around 7 ms, was 30.4 °C. This temperature is significantly under the maximum rated temperature for AWG 22 wire, which is 155 °C

[5]. After 30 ms, the temperature in the copper wire reduced to around 27.9°C. These results show that even though large currents are required to flip the magnetic dipoles in the AlNiCo material, the duration of these high currents is so small that they do not negatively affect the copper wire. Also, the temperatures in the NdFeB and AlNiCo magnets remain virtually unchanged, so heat damage to the magnets is unlikely. As a precaution, the clamp operators should wait several seconds between activations to allow the heat to dissipate.

### ANSYS Optimization Results

Initially, a model of the designed EPMC was created in Ansys to resemble the optimal design from FEMM visualization. The depth of all elements was kept at 50 mm into the page except the AlNiCo magnets and their corresponding steel flanges that were modelled to be a square of side length 45 mm when viewed from above. The coils of wire and the bobbin were not modelled as part of this step, and the surface force density was integrated across the bottom face of the workpiece to obtain the desired clamping force values. The model, as well as the resulting magnetic flux density along the center line and the surface force distribution, is shown below.

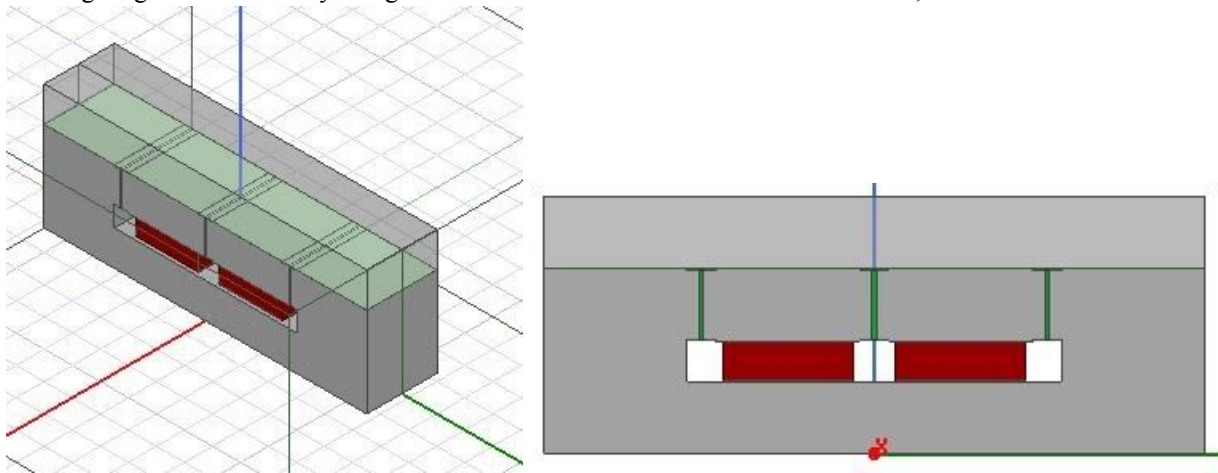


Figure 5 - Isometric and Front View of the EPMC Model in Ansys

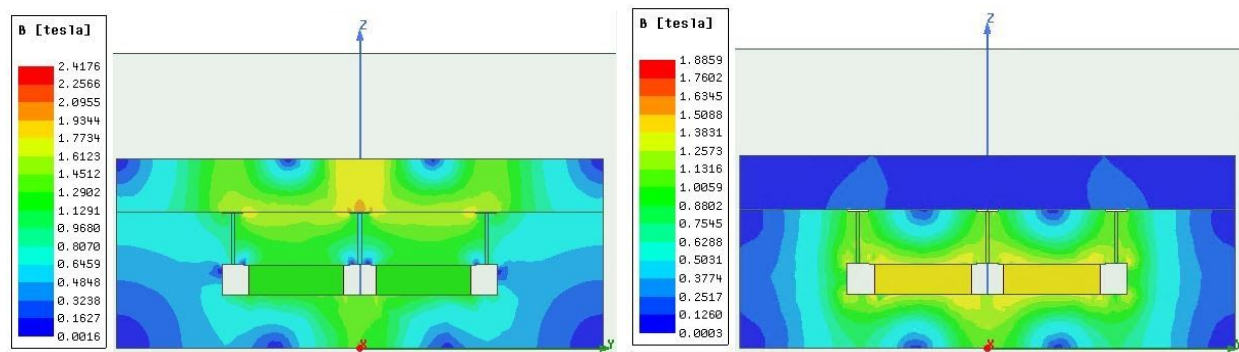


Figure 6 - EPMC Magnetic Flux Density in the “On” and “Off” Configuration

The initial EPMC design resulted in a 1322 lb force in the “on” configuration and residual force of 3.55 lbs when “off”. The initial model mostly met the stated project requirements, but the design was optimized by changing parameters and studying their effect on the force experienced by the workpiece in the “on” and “off” configuration. The “on” and “off” clamping forces were reduced by increasing the width of the steel away from the poles or decreasing the thickness of the NdFeB magnets. The “on” clamping force could be increased while decreasing the “off” residual force by decreasing the vertical distance between the poles and the base, increasing the height of the AlNiCo magnets, or increasing the AlNiCo magnet grade. A front and back steel piece were added to the EPMC case but were soon removed due to creating an unnecessary flux path that reduced the “on” clamping force, as well as reducing the ability to install wiring as needed and ventilate the clamping system.

It was desired that the “off” clamping force would be less than or equal 10 pounds, the “on” clamping force be 1500 pounds or more if possible, and the ratio of the force generated when “on” versus the cost be as high as possible. Weight was not a major design factor as the EPMC will not be regularly moved around and will be

relatively small and light weight compared to other clamp designs. From initial cost estimations, the volume of NdFeB magnets was the most critical parameter due to their unit cost. The width of the steel protruding away from the poles was also studied to understand its effect with the NdFeB magnets. The base and AlNiCo dimensions were set and the AlNiCo magnets were assigned as grade LNG44 to have a relatively high residual magnetic field intensity while simultaneously having a lower intrinsic coercivity, requiring less amp-turns to flip.

Within ANSYS, the dimensions of the NdFeB magnets and the width of the steel piece extruding out the side of the poles were varied in a parametric study, and the forces in the “on” and “off” configuration were evaluated for each variation. All variations with an “off” clamping force greater than 10 pounds were eliminated. This process revealed that making the cross-sectional area of the NdFeB magnets larger decreased the “off” clamping force but also increased the “on” clamping force. Also, the NdFeB magnet thickness had the greatest effect on the amount of clamping force per unit cost, with a small contribution from variation in the width of steel protruding from the poles.

From this parametric study, a thickness of 3.5 mm for the NdFeB magnets and a width of 24 mm protruding from the poles would be optimal when comparing the force produced to the calculated cost. However, another parametric study was conducted varying just these two parameters of interest. The NdFeB magnet thickness was varied from 2.5 mm to 4.5 mm and the width of the steel protruding from the poles was varied from 22 mm to 26 mm. The results for each study are shown below.

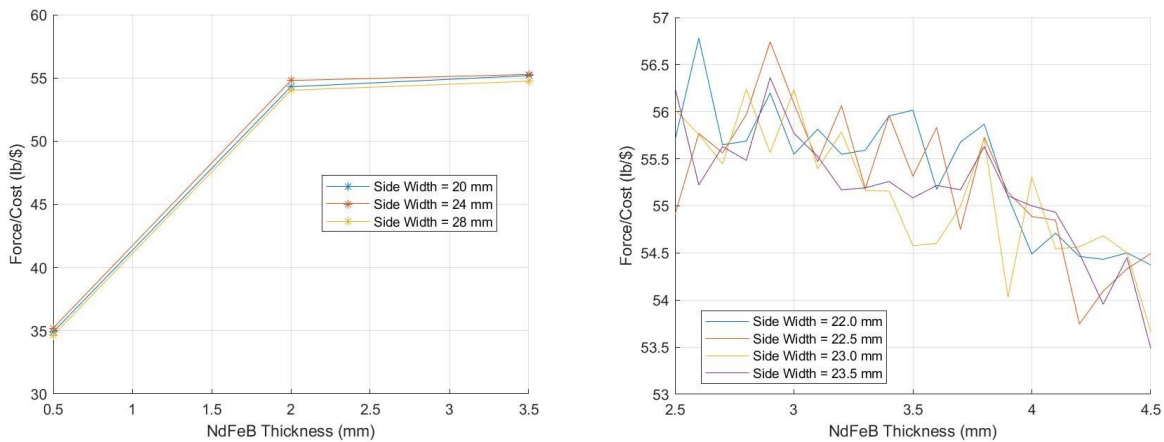


**Figure 7 - “On” Clamping Force per Unit Cost for the 1st and 2nd Parametric Studies**

From these results, a design was selected that would produce an acceptable “off” clamping force, would produce an “on” clamping force around 1500 pounds, and would provide the highest ratio of clamping force over cost possible. From the visualization of the force/cost ratio against the width of the steel, it is tempting to think that the steel width should be decreased as much as possible, but there is a trade off between increased force with decreased cost and keeping the “off” force to an allowable level. The first variations selected had residual “off” forces greater than 10 pounds, so the options were listed in descending order by the ratio of “on” clamping force per unit cost, and the final design was selected as the first one that met this maximum “off” force requirement.

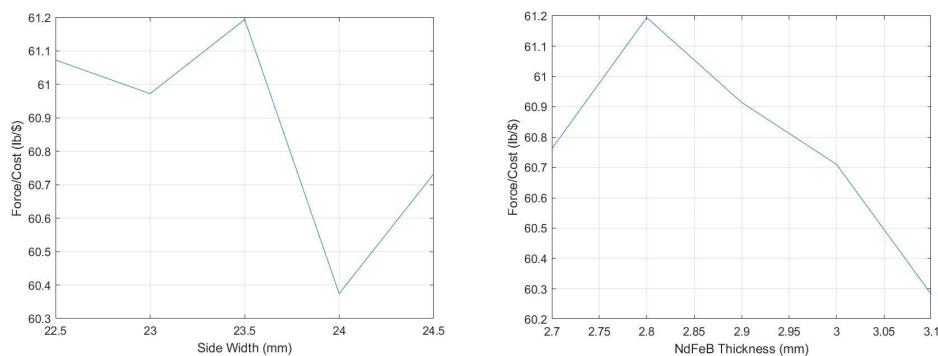


**Figure 8 - “On” Clamping Force per Unit Cost for the Final Parametric Study**

Using the values chosen from the second parametric study, a final parametric study was conducted with the optimum parameters incorporated into the Ansys model. An NdFeB thickness of 2.8 mm and a side width of 23.5 mm produced the flux density distributions below.

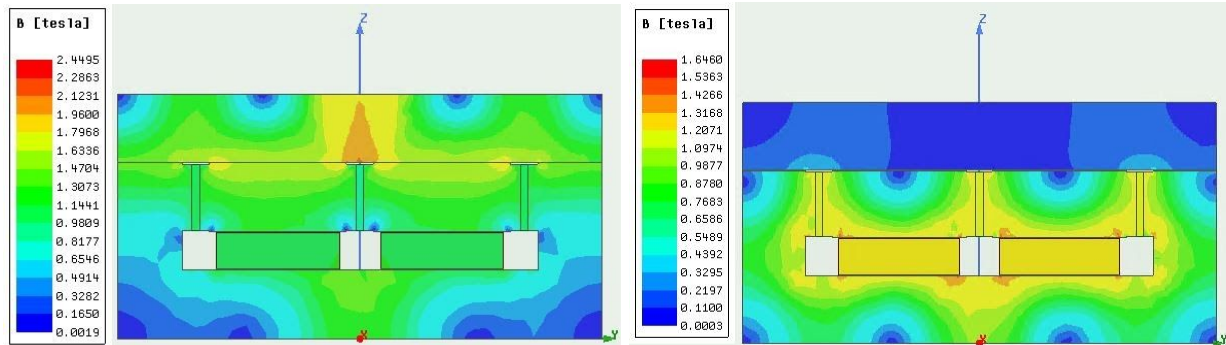


**Figure 9 - Optimized EPMC Magnetic Flux Density in the “On” and “Off” Position**

The performance values of the optimized EPMC design are detailed in the table below.

**Table 3 - Optimized Design Parameters**

“On” Clamping Force [lb]	“Off” Residual Force [lb]	Cost [\$]	Weight [lb]	Unit Force per Unit Cost [lb/\$]	Unit Force per Unit Weight [lb/lb]
1569	9.391	25.64	8.695	61.19	180.4

### Conclusions and Recommendations

Many numerous analysis techniques were used to optimize the design of an Electro-Permanent Magnetic Clamp. MCA was used to develop a rough model that delivered the approximate amount of force. FEMM was used to further refine the design, and wiring and electrical calculations were used to develop a method to effectively flip the device between the on and off configurations. A heat transfer analysis in ANSYS was used to ensure that the magnets and wires in the design do not overheat, and an ANSYS simulation was used to refine the design.

From the theoretical calculations and simulation results, it is possible to create an Electro-Permanent Magnetic Clamp to achieve clamping forces in excess of 1500 lbs with minimal residual force in the “off” position. Although the cost of the bobbin and wire coils were not factored into the cost, the device can be produced at a relatively low cost and weight. From the analysis performed, the AlNiCo magnets should be grade LNG44 and nearly the full bobbin interior volume, with their height being approximately 13.5 mm tall. Also, it is optimal to not include any steel in front or behind the poles, the NdFeB cross-sectional area should be maximized while reducing their overall volume, and the steel case should protrude approximately 23.5 mm from the poles.

Although this analysis could be improved through use of high-power computing, the current results produce an efficient EPMC device. There is also extreme saturation in the AlNiCo magnets when in the “off” position that could be reduced in future designs, but the results have shown that this issue is acceptable as it does not adversely affect the efficiency of the EPMC device.

## References

- [1] K&J Magnetics, Inc. (n.d.). Demagnetization (BH) Curves for Neodymium Magnets. Retrieved from <https://www.kjmagnetics.com/bhcurves.asp>
- [2] Eclipse Magnetics, Ltd. (n.d.). AlNiCo Magnets Data Sheet. Retrieved from <https://www.eclipsemagnetics.com>
- [3] MagWeb. (n.d.). Free BH Curves. Retrieved from <https://magweb.us/free-bh-curves/>
- [4] MagnetShop.com. (2020). Magnet Basics FAQs. Retrieved from <https://www.magnetshop.com/resources/magnet-basics.html#costs>
- [5] BNTECHGO. (2020). BNTECHGO 22 AWG Magnet Wire - Enameled Copper Wire - Enameled Magnet Winding Wire - 3.0 lb - 0.0256" Diameter 1 Spool Coil Natural Temperature Rating 155 Degree C Widely Used for Transformers Inductors. Retrieved from <http://bntechgo.com/bntechgo-22-awg-magnet-wire-enameled-copper-wire-enameled-magnet-winding-wire-3-0-lb-0-0256-diameter-1-spool-coil-natural-temperature-rating-155-widely-used-for-transformers-inductors/>
- [6] Solaris (n.d.). American Wire Gauge Conductor Size Chart. Retrieved from <https://www.solaris-shop.com/content/American%20Wire%20Gauge%20Conductor%20Size%20Table.pdf>

## Appendix A - MCA System of Equations for the On Configuration

$$\begin{aligned} \mathcal{R}_{\text{air}}\Phi_1 + 0.7008 \exp\left(5.155 \frac{\Phi_1}{A_s}\right) L_{s1} + \mathcal{R}_{\text{air}}\Phi_2 + 763,358 \frac{L_r}{A_r} \Phi_5 - 1,030,534 L_r &= 0 \\ 2\mathcal{R}_{\text{air}}\Phi_2 + 0.7008 \exp\left(5.155 \frac{\Phi_6}{A_s}\right) L_{s6} + 763,358 \frac{L_r}{A_r} \Phi_7 - 1,030,534 L_r &= 0 \\ 2 * 284,656 \frac{L_a}{A_a} \Phi_3 - 763,358 \frac{L_r}{A_r} \Phi_7 + 0.7008 \exp\left(5.155 \frac{\Phi_8}{A_s}\right) L_{s8} - 2 * 342,641 L_a + 1,030,534 L_r &= 0 \\ 284,656 \frac{L_a}{A_a} \Phi_3 + 0.7008 \exp\left(5.155 \frac{\Phi_4}{A_s}\right) L_{s4} - 763,358 \frac{L_r}{A_r} \Phi_5 - 342,641 L_a + 1,030,534 L_r &= 0 \\ \Phi_1 - \Phi_2 + \Phi_6 &= 0 \\ \Phi_1 - \Phi_4 - \Phi_5 &= 0 \\ \Phi_3 - \Phi_4 - \Phi_8 &= 0 \\ \Phi_1 - \Phi_2 + \Phi_3 - \Phi_4 + \Phi_7 &= 0 \end{aligned}$$

**Appendix B - On and Off Configuration Force Values**

Width Variation On Forces (kip)

AlNiCo Width	NdFeB Width									
	15mm	16mm	17mm	18mm	19mm	20mm	21mm	22mm	23mm	24mm
30mm	1.07	1.13	1.19	1.25	1.31	1.36	1.41	1.45	1.50	1.54
31mm	1.10	1.16	1.22	1.27	1.33	1.38	1.43	1.47	1.51	1.55
32mm	1.12	1.18	1.24	1.30	1.35	1.40	1.44	1.49	1.53	1.57
33mm	1.15	1.21	1.27	1.32	1.37	1.42	1.46	1.51	1.54	1.58
34mm	1.18	1.23	1.29	1.34	1.39	1.44	1.48	1.52	1.56	1.59
35mm	1.20	1.26	1.31	1.36	1.41	1.46	1.50	1.54	1.57	1.61
36mm	1.23	1.28	1.33	1.38	1.43	1.47	1.51	1.55	1.59	1.62
37mm	1.25	1.30	1.35	1.40	1.45	1.49	1.53	1.57	1.60	1.63
38mm	1.27	1.33	1.38	1.42	1.47	1.51	1.55	1.58	1.62	1.65
39mm	1.30	1.35	1.40	1.44	1.48	1.52	1.56	1.60	1.63	1.66
40mm	1.32	1.37	1.41	1.46	1.50	1.54	1.58	1.61	1.64	1.67
41mm	1.34	1.39	1.43	1.48	1.52	1.55	1.59	1.62	1.65	1.68
42mm	1.36	1.41	1.45	1.49	1.53	1.57	1.60	1.63	1.66	1.69
43mm	1.38	1.43	1.47	1.51	1.55	1.58	1.62	1.65	1.68	1.70
44mm	1.40	1.44	1.49	1.53	1.56	1.60	1.63	1.66	1.69	1.71
45mm	1.42	1.46	1.50	1.54	1.58	1.61	1.64	1.67	1.70	1.72

Width Variation Off Forces (lbf)

AlNiCo Width	NdFeB Width									
	15mm	16mm	17mm	18mm	19mm	20mm	21mm	22mm	23mm	24mm
30mm	3.91	9.45	17.50	28.07	41.17	56.80	74.97	95.69	118.97	144.82
31mm	2.33	6.80	13.79	23.29	35.32	49.88	66.99	86.64	108.85	133.61
32mm	1.21	4.62	10.54	18.98	29.95	43.45	59.49	78.08	99.22	122.91
33mm	0.57	2.90	7.75	15.13	25.04	37.49	52.47	70.00	90.08	112.71
34mm	0.38	1.64	5.43	11.75	20.60	31.99	45.92	62.40	81.42	103.00
35mm	0.66	0.84	3.56	8.82	16.61	26.95	39.84	55.26	73.24	93.76
36mm	1.41	0.50	2.15	6.34	13.08	22.37	34.20	48.59	65.52	85.00
37mm	2.62	0.63	1.19	4.32	10.00	18.23	29.02	42.36	58.25	76.69
38mm	4.31	1.21	0.69	2.74	7.36	14.54	24.28	36.58	51.43	68.84
39mm	6.47	2.26	0.64	1.62	5.17	11.29	19.98	31.24	45.05	61.42
40mm	9.10	3.78	1.06	0.94	3.42	8.48	16.12	26.33	39.11	54.44
41mm	12.23	5.77	1.94	0.72	2.12	6.11	12.69	21.85	33.59	47.89
42mm	15.83	8.23	3.28	0.96	1.27	4.18	9.70	17.81	28.50	41.77
43mm	19.93	11.18	5.10	1.66	0.87	2.70	7.14	14.19	23.84	36.07
44mm	24.51	14.60	7.38	2.82	0.92	1.66	5.03	11.02	19.61	30.80
45mm	29.57	18.51	10.14	4.45	1.43	1.07	3.36	8.28	15.81	25.95

Thickness Variation On Forces (kip)

AlNiCo Thickness	NdFeB Thickness									
	1mm	2mm	3mm	4mm	5mm	6mm	7mm	8mm	9mm	10mm
1mm	0.99	1.09	1.13	1.15	1.16	1.17	1.17	1.18	1.18	1.18
2mm	1.17	1.30	1.36	1.39	1.41	1.42	1.43	1.44	1.44	1.45
3mm	1.24	1.40	1.46	1.50	1.53	1.54	1.55	1.56	1.57	1.58
4mm	1.28	1.45	1.53	1.57	1.60	1.62	1.64	1.65	1.66	1.66
5mm	1.31	1.49	1.57	1.62	1.65	1.68	1.69	1.71	1.72	1.73
6mm	1.33	1.52	1.60	1.66	1.69	1.72	1.74	1.75	1.76	1.77
7mm	1.34	1.54	1.63	1.68	1.72	1.75	1.77	1.79	1.80	1.81
8mm	1.35	1.55	1.65	1.71	1.75	1.78	1.80	1.82	1.83	1.84
9mm	1.36	1.56	1.66	1.72	1.77	1.80	1.82	1.84	1.86	1.87
10mm	1.36	1.57	1.68	1.74	1.78	1.82	1.84	1.86	1.88	1.89
11mm	1.37	1.58	1.69	1.75	1.80	1.83	1.86	1.88	1.90	1.91
12mm	1.37	1.59	1.70	1.76	1.81	1.85	1.87	1.89	1.91	1.93
13mm	1.38	1.60	1.70	1.77	1.82	1.86	1.89	1.91	1.93	1.94
14mm	1.38	1.60	1.71	1.78	1.83	1.87	1.90	1.92	1.94	1.95

Thickness Variation Off Forces (lbf)

AlNiCo Thickness	NdFeB Thickness									
	1mm	2mm	3mm	4mm	5mm	6mm	7mm	8mm	9mm	10mm
1mm	19.75	22.24	23.18	23.67	23.97	24.18	24.33	24.44	24.53	24.60
2mm	20.24	23.00	24.05	24.61	24.95	25.18	25.35	25.48	25.58	25.66
3mm	20.45	23.33	24.43	25.02	25.38	25.62	25.80	25.93	26.04	26.12
4mm	20.56	23.51	24.65	25.25	25.62	25.87	26.05	26.19	26.30	26.38
5mm	20.64	23.63	24.78	25.39	25.77	26.02	26.21	26.35	26.46	26.55
6mm	20.69	23.71	24.88	25.49	25.87	26.13	26.32	26.46	26.57	26.66
7mm	20.72	23.77	24.95	25.57	25.95	26.21	26.40	26.55	26.66	26.75
8mm	20.75	23.82	25.00	25.62	26.01	26.28	26.47	26.61	26.72	26.81
9mm	20.78	23.85	25.04	25.67	26.06	26.32	26.52	26.66	26.77	26.87
10mm	20.79	23.88	25.08	25.71	26.10	26.36	26.56	26.70	26.82	26.91
11mm	20.81	23.91	25.10	25.74	26.13	26.40	26.59	26.74	26.85	26.94
12mm	20.82	23.93	25.13	25.76	26.16	26.42	26.62	26.76	26.88	26.97
13mm	20.83	23.94	25.15	25.78	26.18	26.45	26.64	26.79	26.90	27.00
14mm	20.84	23.96	25.16	25.80	26.20	26.47	26.66	26.81	26.92	27.02